Linear and nonlinear optical properties of ZnO/PMMA nanocomposite films

Bohdan Kulyk, Bouchta Sahraoui, Oksana Krupka, V. Kapustianyk, V. Rudyk, E. Berdowska, S. Tkaczyk, Ivan-V. Kityk

AIP Journal of Applied Physics

Linear and nonlinear optical properties of ZnO/PMMA nanocomposite films

B. Kulyk, B. Sahraoui, O. Krupka, V. Kapustianyk, V. Rudyk, E. Berdowska, S. Tkaczyk, and I. Kityk

Citation: Journal of Applied Physics **106**, 093102 (2009); doi: 10.1063/1.3253745
View online: http://dx.doi.org/10.1063/1.3253745
View Table of Contents: http://scitation.aip.org/content/aip/journal/jap/106/9?ver=pdfcov
Published by the AIP Publishing

Linear and nonlinear optical properties of ZnO/PMMA nanocomposite films

B. Kulyk,[1,a)] B. Sahraoui,[1] O. Krupka,[1,b)] V. Kapustianyk,[2] V. Rudyk,[2] E. Berdowska,[3] S. Tkaczyk,[3] and I. Kityk[4]
[1]*POMA Laboratory, FRE CNRS 2988 UFR Sciences, University of Angers, 2 Boulevard Lavoisier, 49045 Angers Cedex 01, France*
[2]*Scientific-Technical and Educational Center of Low Temperature Studies, Chair of Solid State Physics, Scientific and Educational Center "Fractal," Ivan Franko National University of Lviv, Dragomanova Street, 50, 79005 Lviv, Ukraine*
[3]*Institute of Physics, J. Dlugosz University of Czestochowa, 42-200 Czestochowa, Poland*
[4]*Chemical Department, Silesian Technical University, Stzody Street, 9, 44-100 Gliwice, Poland*

(Received 26 July 2009; accepted 29 September 2009; published online 3 November 2009)

The nanoscale crystals (NCs) of ZnO were embedded into polymethylmethacrylate (PMMA) polymeric matrix and nanocomposite films were prepared by modified spin coating method. The surface of the ZnO/PMMA nanocomposite films has been investigated using atomic force and scanning electron microscopy. The prepared films are highly transparent, the ultraviolet-visible spectra show their high optical quality. The second and third harmonic generation (SHG and THG) studies of ZnO/PMMA nanocomposite films with different concentrations of ZnO NCs were carried out at $\lambda = 1.064$ μm and the effective values of the second and third order nonlinear susceptibilities were estimated to be higher than that of ZnO bulk for the films at low concentration of ZnO NCs. This could indicate that surface effects in ZnO/PMMA nanocomposite films have a dominant role over bulk effects for the SHG and THG processes. © *2009 American Institute of Physics*. [doi:10.1063/1.3253745]

I. INTRODUCTION

Semiconductor materials are of current interest because of their unique electrical and optical properties. In particular, their nonlinear optical (NLO) properties suggest potential application as frequency converters, logic elements in the nanoscale optoelectronic circuitry. Over the past few years, one-dimensional structures with nanoscale diameters such as nanowires, nanorods, and nanotubes have attracted considerable attention due to their peculiar structure characteristics and size effects.[1] These materials often exhibit remarkable mechanical as well as electrical, optical, and electromagnetic properties that are quite different from those of the corresponding bulk materials.[2,3] In the nanometer regime, various quantum mechanical effects, such as an increase of the band gap of a semiconducting material with a reduction of the nanoparticle size, are observed. As a result, there exists a possibility of a continuous tuning of the optical and electronic properties by varying the size of the particles. That is why such materials can be viewed as promising candidates for future applications in the field of catalysis, sensor technology, transistor, electrode materials, logic circuits, and laser working.[1] It is necessary to note that ZnO shows quantum confinement effects in the experimentally accessible range of sizes (less than 7 nm[4–7]). Furthermore, ZnO is a technologically important material with widespread use and there has been much interest in synthesizing ZnO nanocrystals of various sizes in the past few years.[8]

Coherent NLO phenomena such as second and third harmonic generation (SHG and THG) depend explicitly on the crystal lattice structure of the medium, which could yield to a very high polarization selectivity. In addition, the temporal response of the nonresonant harmonic generation is similar to the pulse width of the pump laser (even in femtosecond regime[9]), while the incoherent processes are at least 2–4 order of magnitude slower. Moreover, nonresonant SHG is essentially independent on wavelength below the energy band gap of semiconductor materials, most often including wavelength region typically used in the optical fiber communications. Hence, characterizing the NLO response is crucial for evaluating of the potential applications. However, there are no enough data in the literature concerning the NLO properties of the nanocomposites based on zinc oxide.[2,10]

In this paper, therefore, we investigated the effect of ZnO NCs size and concentration on the NLO properties such as SHG and THG together with the surface morphology and optical absorption investigations. This work is a continuation of our previous work connected with NLO properties in ZnO films and structures.[11–14]

II. EXPERIMENTAL DETAILS

The investigated samples were manufactured on the basis of ZnO nanoparticles embedded into polymethylmethacrylate (PMMA) polymeric matrix. The two types of the nanocomposite films namely ZnO/PMMA 1 and ZnO/PMMA 2 were prepared with various concentrations of ZnO NCs. Their difference consists also in dimensions of ZnO

[a)]Author to whom correspondence should be addressed. Present address: Chair of Solid State Physics, Ivan Franko National University of Lviv, Dragomanova Street, 50, 79005, Lviv, Ukraine. Electronic mail: bohdan_kulyk@yahoo.com.
[b)]Present address: Kyiv Taras Shevchenko National University, Volodymyrska Street, 60, 01033, Kyiv, Ukraine.

nanocrystals (50–100 nm and about 100 nm, respectively). Besides, the samples ZnO/PMMA 1 were additionally treated by laser.

The first type of nanopowder was additionally separated by sizes using nanoporous filter from polystyrrole. The samples before embedding have been annealed in the argon atmosphere during the 5, 10, and 15 h until the electron paramagnetic resonance control showed existence of doubling bonds. The spin coating method was modified by simultaneous heating of the mica substrate and varying the rate of the PMMA solution deposition. We have developed steeply slowing of the deposition process with increasing thickness of the film. Their average thickness was equal about 1 μm, however several deviations existed on the borders of the films. The weight concentration of ZnO nanocrystals in PMMA were 3, 7, 12, and 16%. After evaporation of the tetrahydrofuran during the process of spin coating, the samples were held at fixed temperature about 60 °C and afterward they were steeply cooled. The films prepared by such a way after the full cooling were treated by additional 4 kV/cm and 50 kHz dc electric field and 0.6 GW/cm^2, 337 nm, 10 ns laser field. The band energy calculations have shown that on the interfaces ZnO/PMMA there occurs a large gradient of the electrostatic potential due to difference of the Fermi energy levels. So, to avoid any destruction of the border bonds, additional treatment was repeated after 5–6 days of their preparation. The control by differential scanning calorimetry did not show any presence of phase transformation.

The second type of nanopowder used for nanocomposite films preparation was purchased from Aldrich Co. (<100 nm in size). The glass substrates used were carefully cleaned in a commercial surfactant using ultrasonication. The cleaning procedure was ended by baking in a 200 °C oven for 60 min. Spin coating was used to fabricate nanocomposite films with dispersed ZnO in PMMA. The solution of 1,2,2-trichloroethane containing PMMA 100 g/L and ZnO coated on BK7 glass slides. The weight concentration of ZnO nanocrystals in PMMA were 5, 10, and 15%. The principle of deposition (of the mixture with certain viscosity) is based on a homogeneous spreading out of the solution on the rotating substrate with an angular speed of 1000 rpm during 60 s. Immediately after the deposition, the thin films were cured in a 60 °C oven for 60 min in order to eliminate any remaining solvent.

The thickness of the nanocomposite films was verified by a Dektak surface stylus profiler (Veeco) and was found to be about 1 μm. The atomic force microscopy (AFM) images were recorded in tapping mode at 1 Hz scan rate with a CP Research (Thermomicroscope/Veeco). Scanning electron microscopy (SEM) images were recorded on a JSM-6301F (JEOL) scanning electron microscope with resolution of 1.5 nm, working at 3.0 kV dc acceleration voltages in vacuum ambient. The optical absorption spectra in visible and near ultraviolet (UV) region were measured using a spectrometer Lambda 19 from Perkin Elmer.

SHG and THG measurements were carried out by means of the rotational Maker fringe technique[15] in the transmission scheme (Fig. 1) for the *s*-polarized fundamental beam. A

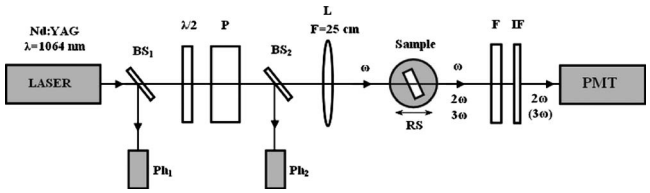

FIG. 1. Experimental setup for SHG and THG measurements: the beam splitters (BS_1, BS_2), the synchronization and control photodiodes (Ph_1, Ph_2), ($\lambda/2$), the Glan polarizer, the converging lens, RS, the filters, IF, and PMT.

y-cut crystalline quartz plate has been used as a reference material for SHG and fused silica plate for THG measurements.

As a fundamental beam, we used the output beam of a Q-switched Nd doped yttrium aluminum garnet laser (model: Quantum Elite) generating at $\lambda = 1064$ nm with 16 ps pulse duration and 10 Hz repetition rate. The incident polarization was selected with a half-wave plate ($\lambda/2$) and polarizer in front of the focusing lens. The intensity at the input face of the sample is assumed to be a Gaussian distribution in space and time. The beam diameter was 0.4 mm at the film and the applied power density was in the range of 5–23 GW/cm^2. The beam was focused onto the sample with lens of 250 mm focal length. A motorized rotation stage (RS) with the mounted sample allowed the variation of the incidence angle with a resolution of 1.0°. After passing the sample, the interference filter (IF) (at 532 nm for SHG or at 355 for THG) was used to cut the pump beam before the photomultiplier. Detector saturation was prevented using linear neutral density filters, whose transmittance value was taken into account during data fitting. The second and third harmonic signals were detected by the photomultiplier tube (PMT) (model: Hamamatsu), which was connected to a boxcar and processed by a computer. A portion of the input beam was selected and measured by a fast photodiode Ph_2 to monitor the input energy. Finally, we got the angular dependences of SHG and THG by rotating the sample toward the normal.

III. RESULT AND DISCUSSION

A. Microscopy analysis

Figure 2 presents AFM and SEM images recorded from ZnO/PMMA 1 (16 wt. %) nanocomposite film. Figure 2(a) shows the AFM image where surface topography was acquired by scanning over the area of 2×2 μm^2. The porous surface of PMMA host system seems suitable for incorporation of ZnO NCs. The magnified SEM image of the top view is shown in Fig. 2(b), the NCs of ZnO are clearly identified inside the porous cells of PMMA and their dimensions are about 50–100 nm or less. Figure 2(c) demonstrates the view of conglomerate of several microns in size created in some cases from the nanocrysatals of zinc oxide that confirms the possible agglomeration of ZnO NCs at their high concentration.

B. Optical absorption measurements

The optical absorption spectra of two types of nanocomposite films were measured and the results are shown in Figs.

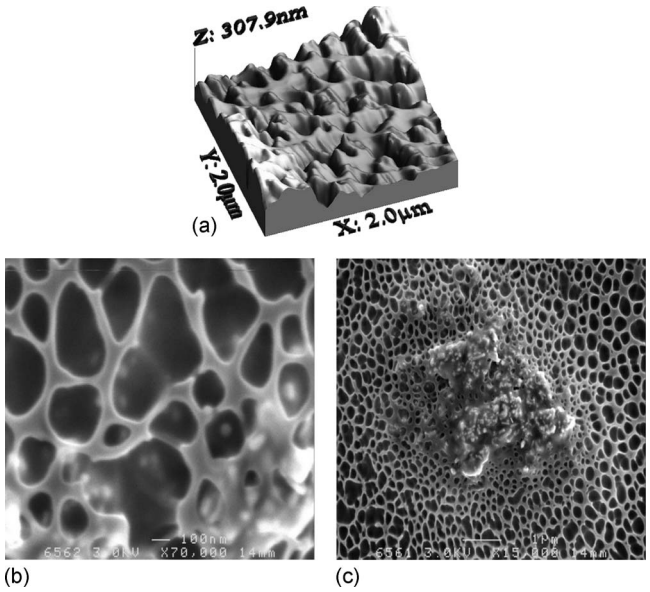

FIG. 2. AFM surface image (a), SEM image of ZnO NCs inside porous PMMA polymeric matrix (b) and SEM image of the agglomerated ZnO NCs (c) in ZnO/PMMA 1 (16 wt %) nanocomposite film.

3 and 4. The ZnO/PMMA films with NCs of lower dimensions demonstrate overall growth of absorption in the region from 300 to 400 nm as compared with pure PMMA film and no exciton absorption peaks characteristic to ZnO are observed. Quite wide dispersion of sizes of ZnO NCs together with their partial agglomeration cause the considerable light scattering in the investigated spectral range preventing observation of the exciton absorption corresponding to ZnO.

Contrary to the previous case, the absorption spectra of ZnO/PMMA nanocomposite films 2 (Fig. 4) clearly demonstrate the absorption peaks at 377 nm (3.29 eV) corresponding to the exciton state in the bulk ZnO.[16] Since the size of ZnO NCs is nearly 100 nm, that is much more than the exciton Bohr radius in ZnO (a_B=2.34 nm) (Ref. 17), we do not observe in our NCs system any shift of the corresponding peak as manifestation of the quantum confinement effect. The intensity of the peaks enhances with increasing of ZnO NCs concentration. The absorption spectra were measured in

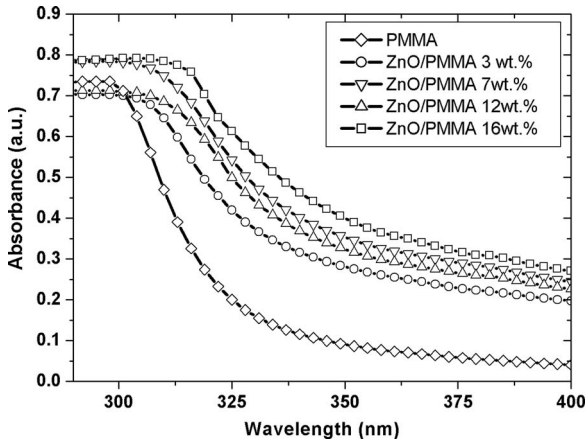

FIG. 3. UV spectra of PMMA and ZnO/PMMA 1 nanocomposite films with different ZnO NCs concentrations: 3, 7, 12, and 16 wt %. The thickness of all films is about 1 μm.

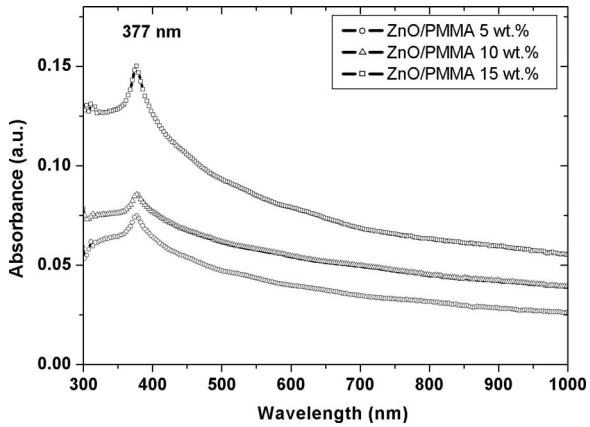

FIG. 4. UV-vis spectra of ZnO/PMMA 2 nanocomposite films with different ZnO NCs concentrations: 5, 10, and 15 wt %. The thickness of all films is around 1 μm.

order to estimate the ideality rate of ZnO/PMMA nanocomposite films and the presence of excitonic peak indicates the high crystallinity of dispersed ZnO NCs inside PMMA.

C. SHG measurements

The SHG measurements were performed by rotational Maker fringe technique for the *s*-polarized fundamental beam. According to the structure of ZnO, which belongs to a hexagonal, noncentrosymmetric space group $P6_3mc$, ZnO nanocrystals should have nonzero second-order NLO efficiency. Figure 5 shows the dependences of SH intensity from ZnO/PMMA nanocomposite films of both types on its ZnO NCs concentrations (and ZnO equivalent thickness). In angular dependences of SHG, a nonzero intensity at normal incidence of fundamental beam was observed due to the various crystalline orientations of ZnO nanocrystals inside film. The observed angular dependences are related to the crystalline symmetry when there is no preferred axis orientation of nanocrystals but only their disorder. Films with higher concentration of ZnO nanocrystals generate stronger second-harmonic signal for the identical input intensities due to the larger interaction thickness of the nonlinear medium. It

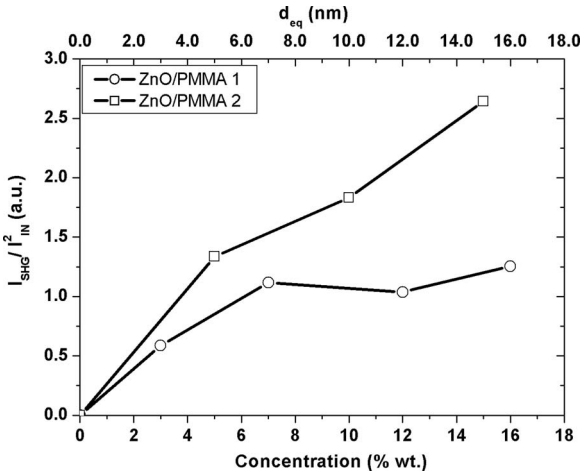

FIG. 5. SH intensity per square of input laser intensity in ZnO/PMMA nanocomposite films on its ZnO NCs weight concentrations and ZnO equivalent thickness.

should also be noted that, even for input intensities in the range of 23 GW/cm^2, no structural change or damage of the samples occurred.

For an isotropic, absorbing nonlinear material, deposited on the substrate and neglecting reflections, we have the following expression for transmitted SH intensity:[15]

$$I_{2\omega}^{s\to p}(\theta) = \frac{128\pi^5}{c\lambda^2}\frac{[t_{af}^{1s}]^4[t_{fs}^{2p}]^2[t_{sa}^{2p}]^2}{n_{2\omega}^2\cos^2\theta_{2\omega}} I_\omega^2 (L\chi_{eff}^{(2)})^2 \exp[-2(\delta_1 + \delta_2)]\frac{\sin^2\Phi + \sinh^2\Psi}{\Phi^2+\Psi^2}, \quad (1)$$

where I_ω is the intensity of the pump wave, λ is the wavelength of pump wave, $\chi_{eff}^{(2)}$ is the effective second order nonlinear susceptibility, L is the material thickness, and t_{af}^{1s}, t_{fs}^{2p}, t_{sa}^{2p} are the Fresnel transmission coefficients (air-film-substrate-air system) for fundamental and SHG beams. The phase angle Φ and Ψ can be expressed as[15]

$$\Phi = \frac{2\pi L}{\lambda}(n_\omega \cos\theta_\omega - n_{2\omega}\cos\theta_{2\omega}), \quad (2)$$

$$\Psi = \delta_1 - \delta_2 = \frac{2\pi L}{\lambda}\left(\frac{n_\omega\kappa_\omega}{\cos\theta_\omega} - \frac{n_{2\omega}\kappa_{2\omega}}{\cos\theta_{2\omega}}\right), \quad (3)$$

where θ_ω, $\theta_{2\omega}$ are the fundamental and generated beams refractive angles determined by Snell's law: $\sin\theta = n_\omega \sin\theta_\omega = n_{2\omega}\sin\theta_{2\omega}$, n_ω, $n_{2\omega}$ and κ_ω, $\kappa_{2\omega}$ are the refractive indices and extinction coefficients of the nonlinear material at frequencies ω and 2ω. The refractive indices of ZnO have been evaluated according Sellmeier model.[18,19]

In our case, the nonlinear material is neither bulk nor film, it is crystalline particles inside the polymeric film. In order to make the calculations of the nonlinear susceptibility of ZnO NCs, we used the notion of equivalent thickness of nonlinear medium inside PMMA as the thickness, which could have ZnO nanocrystals without host PMMA. It has been used in Eq. (1) instead of ordinary thickness and can be expressed as

$$d_{ZnO}^{eq} = \frac{\%wt_{ZnO}}{100 - \%wt_{ZnO}}\frac{\rho_{PMMA}}{\rho_{ZnO}} d_{PMMA+ZnO}, \quad (4)$$

where ρ_{PMMA}, ρ_{ZnO} are densities of PMMA and ZnO, respectively, $\%wt_{ZnO}$ is the weight concentration of ZnO nanocrystals inside a polymeric matrix, $d_{PMMA+ZnO}$ is the thickness of ZnO/PMMA nanocomposite film. As one can see, the intensity of SH (Fig. 5) increases with growth of ZnO amount in both nanocomposites but the shape of these dependences is not quadratic as predicted by NLO theory where the SHG depends quadratically on the thickness of a nonlinear medium [Eq. (1)]. Such a behavior can be connected with the creation of the large agglomerates from ZnO nanocrystals at high enough their concentration that reduce the overall SHG response interacting with fundamental laser beam.

A considerable contribution to the nonlinear effects can stem from a photothermal heating, which can be considered as a result of energy transfer from a heated nanoparticle to the entire medium. Although the response time of this process is much longer in comparison with pulse duration (it is determined by the ratio of the focused laser beam radius to the value of the sound velocity in the dielectric matrix)[20] but high optical transparency of both ZnO-nanoparticles and PMMA matrix diminish the manifestations of the thermal effect. A cumulative thermal effect did not take place in our experiments because the low repetition rate of the laser has been used. Besides, in our experiments, the role of photoinduced Kerr effect, photoinduced anharmonic effect cannot be neglected. Thus, the measurements are a superposition of both local reconstructed NCs surfaces as well as the other effects.

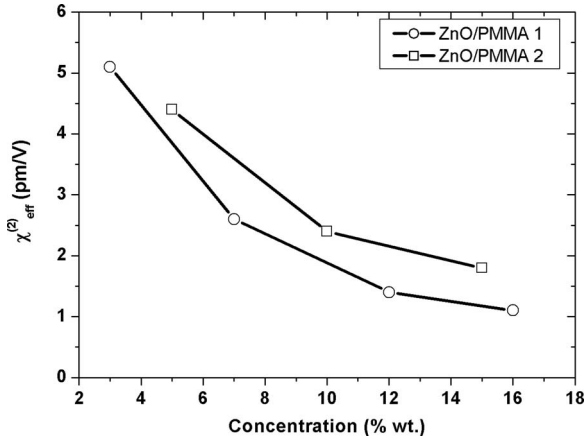

FIG. 6. Calculated values of the effective second-order NLO susceptibilities of ZnO NCs of different size as a function of ZnO NCs concentration.

To estimate the absolute value of the effective second-order nonlinear susceptibility of the ZnO/PMMA nanocomposite films, we used the Eq. (1) and calculations were made at the normal angle of incidence. Figure 6 shows the obtained effective values of the second order NLO susceptibility of ZnO/PMMA nanocomposites plotted versus ZnO weight concentration. The decrease of $\chi_{eff}^{(2)}$ is observed for both types of films. At the ZnO NCs concentration of 5% wt. and less, the values of $\chi_{eff}^{(2)}$ are higher than that of ZnO bulk which is about 2.5 p.m./V for the same experiment geometry in *c*-oriented ZnO crystal.[21] It is necessary to note that the NLO response of the films embedded with larger ZnO nanocrystals ($\sim$100 nm) was found to be a little higher than those for the films with smaller ZnO nanocrystals ($<$100 nm). If the dimensions of nanocrystals are small in comparison with their coherent length ($d \ll l_{coh}$) in any nanocrystal orientation, the interaction will be always phase matched since in such small distance the phase shift is negligible. In this case, the SH power will be proportional to the radius of the nanoparticle. Thus, the efficiency of the nonlinear interaction quickly increases with growth of the nanoparticle radius but at the expense of decrease of nanoparticles this increase is a little compensated.[22] In materials which do not allow phase matched SHG at the dimensions of particles larger than their average coherent length, the power of SH changes inversely to the particles radius.

As one can expect, the $\chi_{eff}^{(2)}$ is larger than that of bulk material when the surface effects give a larger contribution than the volume effects due to the decrease of the characteristic material size to nanoscale. Such a behavior was ob-

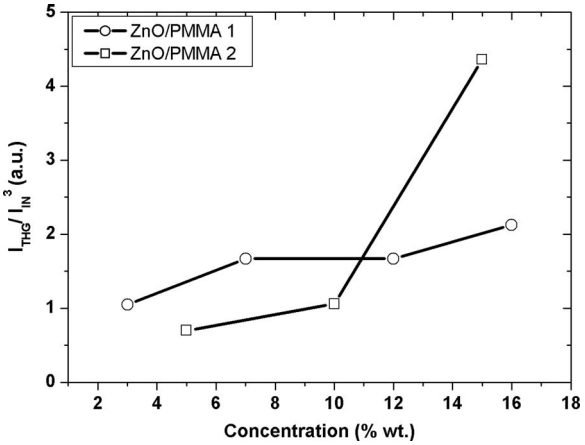

FIG. 7. TH intensity per cube of input laser intensity in ZnO/PMMA nanocomposite films as a function of ZnO NCs weight concentrations.

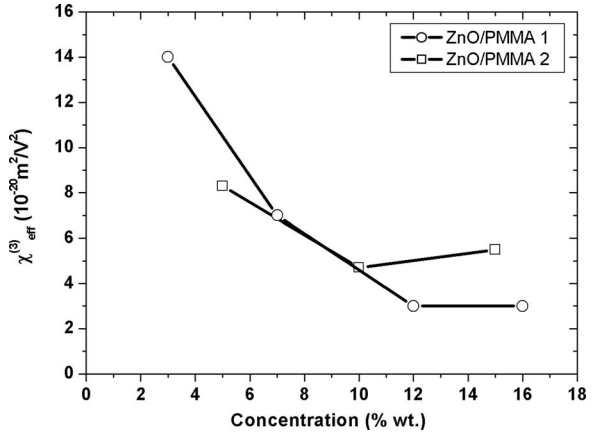

FIG. 8. Calculated values of the effective NLO susceptibilities of third order in ZnO/PMMA films with different concentrations of ZnO nanocrystals.

served in our samples at low ZnO concentration. Increasing of ZnO concentration leads to the opposite effect due to the strong agglomeration of ZnO nanoparticles, redistribution of their density within the polymeric matrix that generate the extraneous processes like light scattering.

D. THG measurements

The third-order optical nonlinearities of ZnO nanocrystals were investigated by THG technique in order to study the effect of particle dimensions on the cubic nonlinear response. Figure 7 shows the dependences of THG intensities in ZnO/PMMA films on the ZnO concentration. In both films, the THG intensity increases with concentration. Besides, for the films containing larger ZnO NCs (~100 nm) this increase was found to be more pronounced. The THG originates from the nanocomposite ZnO together with the PMMA matrix, since the THG process can occur in any material regardless of its symmetry.

According to the work of Wang *et al.*,[23] the intensity of the THGs in a nonlinear film upon a substrate in air ambient neglecting the scattering is given by the following equation:

$$I^{3\omega} = \frac{64\pi^4}{c^2}\left|\frac{\chi_s^{(3)}}{\Delta\varepsilon_s}\right|(I^{\omega})^3 |e^{i(\psi_s^{3\omega}+\psi_f^{\omega})}[T_1(e^{i\Delta\psi_s}-1) + \rho e^{i\phi}T_2(1-e^{-i\Delta\psi_f})] + C_{\text{air}}|^2, \quad (5)$$

where

$$\rho e^{i\phi} = \left|\frac{\chi_f^{(3)}}{\Delta\varepsilon_f}\right| / \left|\frac{\chi_s^{(3)}}{\Delta\varepsilon_s}\right|, \quad (6)$$

$\chi_f^{(3)}$, $\chi_s^{(3)}$ are the third order effective nonlinear susceptibilities of the film and substrate, $\Delta\varepsilon_f$, $\Delta\varepsilon_s$ are the dispersions of the dielectric constants, C_{air} is the contribution of air, $\Delta\Psi_s$, $\Delta\Psi_f$ are the phase angles in substrate and film, respectively. The detailed description is given in the work of Kulyk *et al.*[11]

Using Eq. (5), we calculated the effective values of the cubic nonlinear susceptibilities for the films with diverse concentration of ZnO nanocrystals. Figure 8 demonstrates the ZnO NCs concentration dependences of $\chi_{\text{eff}}^{(3)}$. Similar to the quadratic susceptibility, $\chi_{\text{eff}}^{(3)}$ decrease with ZnO NCs concentrations and at the concentration more than 10% wt. the ZnO nanocrysatals with size of about 100 nm are characterized by higher third order nonlinearity. These values are one-two orders of magnitude higher than that of ZnO bulk crystal [$\chi_{\text{ZnO bulk}}^{(3)} = 1.7\times10^{-21}$ m^2/V^2] (Ref. 24) and correlate fairly well with those obtained for the nanostructured ZnO films.[11–14]

The film structure is believed to be tightly correlated with the nonlinearity. In the case when the structure has no preferred crystalline orientation and consists of the dispersed particles of nanosizes comparative with Bohr radius, an enhancement of some properties like optical nonlinearities should be observed. Indeed, we have obtained quite high second and third order NLO response for nanodispersed ZnO. The reason of $\chi_{\text{eff}}^{(3)}$ enhancement could be related to the fact that the electric field amplitude of an incident laser beam becomes nonuniformly distributed between the two constituents of the composite, and under suitable conditions the electric field strength within the more nonlinear constituent will exceed the spatially average field strength.[25] Under these conditions, the effective third-order susceptibility $\chi_{\text{eff}}^{(3)}$ of the composite can exceed that of either of its constituents.

IV. CONCLUSIONS

We have demonstrated the properties of the ZnO/PMMA nanocomposite films for second and THG of picosecond optical pulses. It has been shown that SHG as well as THG signal increases with ZnO NCs concentration. Nevertheless, the concentration dependences of NLO susceptibilities have inverse character, i.e., $\chi_{\text{eff}}^{(2)}$ and $\chi_{\text{eff}}^{(3)}$ decrease with ZnO NCs concentration. The nanoparticles of ZnO embedded into PMMA show quite high second and third order nonlinearity at low ZnO NCs concentration and high resistance to the intensive laser light which make this material very interesting for other investigations and further possible application.

ACKNOWLEDGMENTS

The authors acknowledge the Service Commun d'Imageries et Analyses Microscopiques of University of Angers for performing SEM and AFM measurements. This work is supported by INTAS (Grant No. 06-1000019-6137)

and Ministry of Science and Education of Ukraine (Project "Physics and Chemistry of the Nanosystem").

[1]M. S. Dresselhaus, Y. M. Lin, O. Rabin, A. Jorio, A. G. Souza Filho, M. A. Pimenta, R. Saito, G. Samsonidze, and G. Dresselhaus, Mater. Sci. Eng., C **23**, 129 (2003).
[2]Q. Chang, H. Ye, and Y. Song, Colloids Surf., A **298**, 58 (2007).
[3]B. S. Zou and V. V. Volkov, Chem. Mater. **11**, 3037 (1999).
[4]R. Viswanatha, S. Sapra, B. Satpati, P. V. Satyam, B. N. Devb, and D. D. Sarma, J. Mater. Chem. **14**, 661 (2004).
[5]D. Sun, N. Miyatake, and H.-J. Sue, Nanotechnology **18**, 215606 (2007).
[6]C.-H. Hung and W.-T. Whang, J. Mater. Chem. **15**, 267 (2005).
[7]S. Li, M. S. Toprak, Y. S. Jo, J. Dobson, D. K. Kim, and M. Muhammed, Adv. Mater. **19**, 4347 (2007).
[8]L. Guo, S. H. Yang, C. L. Yang, P. Yu, J. N. Wang, W. K. Ge, and G. K. L. Wong, Chem. Mater. **12**, 2268 (2000).
[9]U. Griebner, R. A. Kaindl, T. Elsaesser, and W. Seeber, Appl. Phys. B: Lasers Opt. **67**, 757 (1998).
[10]B. Krishnan, L. Irimpan, V. P. N. Nampoor, and V. Kumar, Physica E (Amsterdam) **40**, 2787 (2008).
[11]B. Kulyk, Z. Essaidi, J. Luc, Z. Sofiani, G. Boudebs, B. Sahraoui, V. Kapustianyk, and B. Turko, J. Appl. Phys. **102**, 113113 (2007).
[12]B. Kulyk, Z. Essaidi, V. Kapustianyk, B. Turko, V. Rudyk, M. Partyka, M. Addou, and B. Sahraoui, Opt. Commun. **281**, 6107 (2008).
[13]B. Kulyk, B. Sahraoui, V. Figà, B. Turko, V. Rudyk, and V. Kapustianyk, J. Alloys Compd. **481**, 819 (2009).
[14]Z. Sofiani, B. Sahraoui, M. Addou, R. Adhiri, M. A. Lamrani, L. Dghoughi, N. Fellahi, B. Derkowska, and W. Bala, J. Appl. Phys. **101**, 063104 (2007).
[15]W. N. Herman and L. M. Hayden, J. Opt. Soc. Am. B **12**, 416 (1995).
[16]Ü. Özgür, Ya. I. Alivov, C. Liu, A. Teke, M. A. Reshchikov, S. Doğan, V. Avrutin, S.-J. Cho, and H. Morkoç, J. Appl. Phys. **98**, 041301 (2005).
[17]K. F. Lin, H. M. Cheng, H. C. Hsu, L. J. Lin, and W. F. Hsieh, Chem. Phys. Lett. **409**, 208 (2005).
[18]Y. C. Liu, J. H. Hsieh, and S. K. Tung, Thin Solid Films **510**, 32 (2006).
[19]H. Yoshikawa and S. Adachi, Jpn. J. Appl. Phys. **36**, 6237 (1997).
[20]A. I. Ryasnyanskiy, B. Palpant, S. Debrus, U. Pal, and A. Stepanov, J. Lumin. **127**, 181 (2007).
[21]M. J. Weber, *Handbook of Optical Materials* (CRC Press, Boca Raton, 2003), p. 499.
[22]F. Zernike and J. E. Midwinter, *Applied Nonlinear Optics* (John Wiley, New York, 1973), p. 199.
[23]X. H. Wang, D. P. West, N. B. McKeown, and T. A. King, J. Opt. Soc. Am. B **15**, 1895 (1998).
[24]C. Y. Liu, B. P. Zhang, N. T. Binh, and Y. Segawa, Appl. Phys. B: Lasers Opt. **79**, 83 (2004).
[25]G. L. Fischer, R. W. Boyd, R. G. Gehr, S. A. Jenekhe, J. A. Osaheni, J. E. Sipe, and L. A. Weller-Brophy, Phys. Rev. Lett. **74**, 1871 (1995).